Computational Materials Science 50 (2011) 2886–2890

Contents lists available at ScienceDirect

Computational Materials Science

journal homepage: www.elsevier.com/locate/commatsci

Sign-changeable spin-filter efficiency and giant magnetoresistance in seamless graphene nanoribbon junctions

Chengyong Xu, Linze Li, Hong Li, Rui Qin, Jiaxin Zheng, Guangfu Luo, Qihang Liu, Xin Yan, Lili Yu, Jing Lu *, Zhengxiang Gao

State Key Laboratory of Mesoscopic Physics and Department of Physics, Peking University, Beijing 100871, PR China

ARTICLE INFO

Article history:
Received 13 November 2010
Received in revised form 26 April 2011
Accepted 1 May 2011
Available online 24 May 2011

Keywords:
Graphene nanoribbon
Spin-filter efficiency
Magnetoresistance
Quantum transport calculation

ABSTRACT

Sign-changeable spin-filter efficiency is predicted in both the ferromagnetic and antiferromagnetic configurations of a zigzag graphene nanoribbon bridging two half-planar graphene electrodes from *ab initio* quantum transport calculations. By changing edge spin-polarization configuration, we obtain giant room-temperature magnetoresistance, which is one order of magnitude larger than the maximum experimental results.

1. Introduction

Graphene has been attracting much attention as a candidate material for spintronics because of its long spin relaxation time and length [1–6] due to a small spin–orbit coupling of carbon atoms. The most popular existing spintronic devices are spin-valves. Spin-valves based on graphene have been experimentally fabricated recently. A 10% magnetoresistance (MR) is observed in a spin-valve with a graphene wire contacted by two soft magnetic NiF electrodes at 300 K [7]. A spin-valve consisting of a graphene flake and ferromagnetic electrodes shows a 12% MR at 7 K and the signals persist up to 60 K when an ultrathin MgO tunnel barrier is inserted at the graphene/electrode interface [8]. MR decreases with the increasing bias voltage and oscillates with the gate voltage. Improving MR of graphene-based spin valve is desirable for the sake of wide application in spintronics.

Pure infinite graphene has no magnetism. Zigzag-edged graphene nanoribbons (ZGNRs), however, have magnetic moment on the two edges. Spin in each edge of ZGNRs is ferromagnetically (FM) coupled [9–11]. The ground states of ZGNRs have the two edges antiferromagnetically (AFM) coupled, and a gap is opened in the band structure. FM coupling between the two edges of ZGNRs produces a metallic state, which is slightly higher in energy (about a few meV per edge atom) than the ground state. The parallel spin polarization of the two edges can be stabilized by applying an experimentally accessible magnetic field. Two schemes are proposed to fabricate spin-valve from ZGNRs. The first-type spin-valve uses a ferromagnetic ZGNR connected to two ferromagnetic electrodes and functions via changing the relative direction of the local magnetic field applied on the electrodes [12,13]. The current in the parallel configuration is much larger than that in the antiparallel configuration. Giant MR (GMR) up to 1 million percent (optimistic definition) is predicted for H-saturated ZGNR device [12] and 1 billion percent is predicted for bare ZGNR device [13] at small bias from *ab initio* transport calculations. The additional orbital symmetry matching besides traditional spin matching in ZGNRs is responsible for this striking GMR. Nearly perfect spin-filtering efficiency (SFE) is also predicted for the first-type ZGNR-based spin-valve in the antiparallel configuration [12,13]. This theoretical prediction has been corroborated by recent experiment which gives nearly 100% (pessimistic definition) MR [14]. The second-type spin-valve uses an antiferromagnetic ZGNR connected to two metal electrodes and functions by applying a magnetic field on the ZGNR to transform the semiconducting antiferromagnetic state into the metallic ferromagnetic state [15]. The conductance in the FM configuration is much larger than that in the AFM configuration, and the resulting MR from the Hubbard model is nearly 100% (pessimistic definition) [15] at zero bias voltage.

Note that the actual spin-valve device works under finite bias, and bias usually affects MR significantly. It is necessary to examine the MR behavior of the second-type ZGNR-based spin-valve under finite bias. In this work, we present *ab initio* study of transport properties of the second-type ZGNR-based spin valve under finite voltages. Very recently, graphene nanoribbon seamlessly connected to graphene has been fabricated in experiment [16]. To mimic the

* Corresponding author.
E-mail address: jinglu@pku.edu.cn (J. Lu).

0927-0256/$ - see front matter © 2011 Elsevier B.V. All rights reserved.
doi:10.1016/j.commatsci.2011.05.004

structure mentioned above, we adopt two-dimensional semi-infinite graphene layer as electrodes, instead of using metallic graphene nanoribbons [10,12,17,18] as electrodes. We find that the currents of both the FM and AFM configurations of a ZGNR in this device are actually spin polarized and remarkably the sign of SFE changes with bias. The bias-induced reversal of the spin polarization has potential applications in logic spintronic devices. Room-temperature GMR (optimistic definition) up to several thousand percent at finite bias is predicted, which is one order of magnitude larger than the previously reported experimental values [19–22].

2. Model and method

The two-probe model of H-terminated ZGNRs connected to semi-planar graphene is as shown in Fig. 1. The separation between two adjacent ZGNRs in the same plane is 11.9 Å, and the separation between two adjacent planes is 10 Å. A ZGNR is denoted as *N*-ZGNR according to its width, where *N* is the number of the lateral zigzag chains. The examined H-terminated ZGNRs have widths of $N = 3–8$, or width w_{ribbon}=7–18 Å. The lengths of the central ZGNRs we studied are the same, being $l_{\text{ribbon}} = 28.3$ Å. Atom positions in the central region and surface layers are relaxed based on the density functional theory (DFT) method implemented in the ATK [23–25] code. Quasi-Newton method with force tolerance of 0.05 eV/Å is used. Spin-polarized quantum transport properties are computed based on the DFT coupled with the non-equilibrium Green's function (NEGF) formalism implemented in the ATK [23–25] code. The *k*-points of integration over the Brillouin zone are set to be $10 \times 1 \times 500$ [26]. Single-zeta basis and GGA-PBE [27] exchange correlation functional are employed throughout the calculations. Self-consistent calculations are performed with mixing rate of 0.1, atomic mesh cutoff of 150 Rydberg, and tolerance of 10^{-5}. The electrode temperature is set to 300 K in the calculation.

The spin-polarized current I_σ under bias V_{bias} is calculated with the Landauer-Büttiker formula [28]:

$$I_\sigma(V_{\text{bias}}) = \frac{e}{h}\int\{T_\sigma(E, V_{bias})[f_L(E, V_{\text{bias}}) - f_R(E, V_{\text{bias}})]\}dE, \quad (1)$$

where $T_\sigma(E, V_{\text{bias}})$ is the spin-polarized transmission probability, $f_{L/R}(E, V_{\text{bias}})$ denotes the Fermi–Dirac distribution function of the left (L)/right (R) electrode, and σ represents the spin.

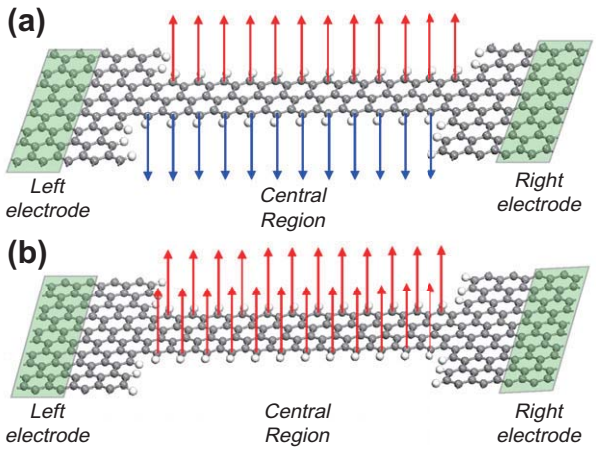

Fig. 1. Schematic models of H-terminated ZGNR connected to two semi-infinite graphene sheets at the armchair edges. (a) The 3-ZGNR in the AFM configuration. (b) The 4-ZGNR in the FM configuration. The coupling of the two edges can be controlled by applying or removing magnetic field. The red/blue arrow denotes up/down spin on edge atoms. (For interpretation of the references to colour in this figure legend, the reader is referred to the web version of this article.)

SFE at finite bias is defined as:

$$\text{SFE} = \frac{I_{\text{up}} - I_{\text{down}}}{I_{\text{up}} + I_{\text{down}}}, \quad (2)$$

where I_{up} and I_{down} are the currents of up and down spin respectively.

3. Results and discussion

The currents of the ZGNRs in the both AFM and FM configurations are spin polarized. Fig. 2a shows the contrast between the spin-up and spin-down currents of the AFM-coupled 3-ZGNR and the FM-coupled 4-ZGNR. The contrast between the spin-up and spin-down currents of other ZGNRs in both the AFM and FM configurations is provided in Fig. S1 of Supplementary Information.

The asymmetrical ZGNRs (*N* is odd) in the AFM configuration have much larger absolute SFEs (Fig. 2b) than those (Fig. 2c) of the symmetrical ZGNRs (*N* is even) at finite bias although the energy band structures of the symmetrical and asymmetrical ZGNRs are almost the same [11,29,30]. Generally, the narrower the asymmetrical ZGNR, the higher is the absolute SFE. At a voltage of lower than 0.5 V, the SFEs of the asymmetrical ZGNRs in the AFM configuration are negative, indicating that the spin-down electrons dominate the spin-up ones. The maximum absolute SFEs are 77%, 47%, and 24% for the 3-, 5-, and 7-ZGNRs at 0.2, 0.15, and 0.1 V, respectively.

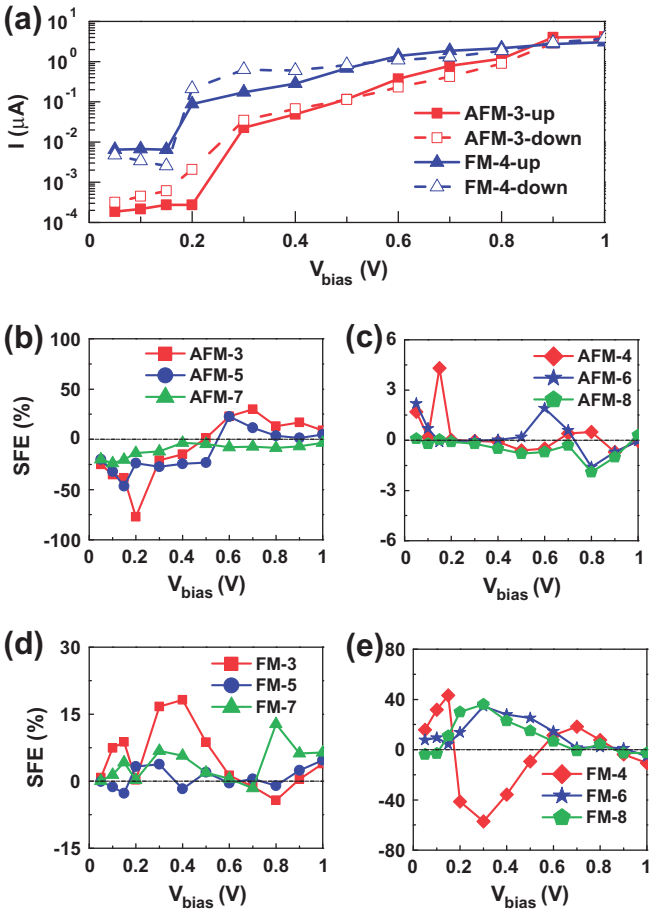

Fig. 2. (a) Spin-resolved *I–V* characteristics of the AFM-coupled 3-ZGNR and FM-coupled 4-ZGNR. (b) Bias-dependent SFEs of the asymmetrical ZGNRs in the AFM configuration. (c) Bias-dependent SFEs of the symmetrical ZGNRs in the AFM configuration. (d) The same as (b), but in the FM configurations. (e) The same as (c), but in the FM configuration. Positive/negative SFE represents that the current is dominated by up/down spin electrons.

However, when the voltage reaches 0.6 V, the SFEs of the AFM-coupled 3- and 5-ZGNRs change their signs from negative (the spin-down electrons dominate) to positive (the spin-up electrons dominate) value while that of the 7-ZGNR remains negative. The bias-induced reversal of the spin polarization has potential applications in logic spintronic devices and it has been reported recently for the inorganic Fe/GaAs(0 0 1) interface [31,32] due to an interfacial minority-spin resonant state [33]. Wang et al. also predicted that the sign of the spin current of the Au–$Fe_5Cp^*_4$–Au system can be altered by changing the bias [34]. The maximum positive SFE is 30% (23%) for the 3-ZGNR (5-ZGNR) at 0.7 V (0.6 V). As the voltage is higher, the SFEs of the 3-, 5-, and 7-ZGNR decay rapidly. Sign switch of SFE with the voltage is also available for the symmetrical ZGNRs in the AFM configuration.

In the FM configuration, the asymmetrical ZGNRs generally have smaller absolute SFEs (Fig. 2d) than those (Fig. 2e) of the symmetrical ZGNRs at finite bias. The FM-coupled 3-ZGNR has moderate SFEs with the maximum value of 18% at 0.4 V, while the 5- and 7-ZGNRs have small SFEs. The dominant spin of the asymmetrical ZGNRs is up spin. The sign of SFEs of the FM-coupled 4-ZGNR oscillates with the voltage. Its SFEs are positive at the voltages of no more than 0.15 V with the maximum of 43% at 0.15 V. As the voltage increase from 0.2 to 0.5 V, the SFEs change to negative value with the absolute maximum of 57% at 0.3 V. The SFE restores positive value as the voltage reaches 0.6 V. The FM-coupled 6- and 8-ZGNR basically have positive SFEs at various voltages. The maximum SFEs of the 6- and 8-ZGNRs are 34% and 38%, respectively, at 0.3 V.

To understand the origin of SFE, it is necessary to investigate the transmission spectrum and the spatially-resolved local density of states (LDOS). We take the FM-coupled 4-ZGNR as an example. Fig. 3a–c show the spin-resolved transmission spectra of the FM-coupled 4-ZGNR at V_{bias} = 0.3 V, 0.7 V, and 1.0 V, respectively. The transmission coefficients of the spin-down electrons are always higher than those of the spin-up ones within the bias window at V_{bias} = 0.3 V, a result in agreement with a large negative SFE (-57%) under this bias. The LDOSs at the Fermi level (E_f) for the spin-up and spin-down electrons under V_{bias} = 0.3 V are shown in Fig. 3d and g, respectively. The LDOS of the spin-down electrons in the central region is apparently larger than that of spin-down electrons. At V_{bias} = 0.7 V, the spin-up and spin-down electrons dominates alternately the transmission spectra, and the spin-up ones slightly dominates on the whole. This is in agreement with a slight positive SFE (18%) at this bias. The LDOSs at E_f for the spin-up and spin-down electrons under V_{bias} = 0.7 V are shown in Fig. 3e and h, respectively. The LDOS near the central line of the nanoribbon of the spin-up electrons is slightly larger than that of the spin-down ones, a result consistent with the somewhat higher transmission coefficient at E_f for the spin-up electrons than the spin-down ones. At V_{bias} = 1.0 V, contrary to the case of V_{bias} = 0.7 V, the contrast of spectra (Fig. 3c) and LDOSs (Fig. 3f and i) of spin-up and spin-down electrons shows the opposite dominance, spin-down over spin-up electrons. The dominance is in accord with the slight negative SFE (−11%) at this bias. In a whole, the sign of the SFE of FM-coupled 4-ZGNR oscillates with the voltage.

The total currents in the FM configuration are much larger than those in the AFM configuration for all the checked ZGNRs. Fig. 4a and b show the current contrast of the FM and AFM configurations of the 3- and 4-ZGNR, respectively. The current contrasts between the FM and AFM configurations of other ZGNRs are provided in Fig. S2 of Supplementary information. In Fig. 4c, we plot the transmission spectra contrast of the 4-ZGNR at 0.3 V between the FM and AFM configurations (the transmission spectra of 3-ZGNR at 0.3 V are almost the same as that of 4-ZGNR). Consistent with the larger current in the FM configuration, the transmission coefficients in the FM configuration are much larger than those in the AFM configuration throughout the bias window. The difference in conducting mechanism (metallic versus tunneling) is also reflected from the LDOS at E_f as shown in Fig. 4d and e. The LDOS of the FM configuration is much larger than that in the AFM configuration.

MR is calculated according to the optimistic definition:

$$\mathrm{MR} = \frac{I_{\mathrm{FM}} - I_{\mathrm{AFM}}}{I_{\mathrm{AFM}}} \tag{3}$$

where I_{FM} (I_{AFM}) is the current of the junctions in the FM (AFM) configuration. Fig. 5 shows MR against bias of different-width ZGNRs. The six ZGNRs have oscillating room-temperature GMR of hundreds to thousands of percent at lower bias (lower than 0.6 V), and their GMRs decay with the bias at higher bias. 4- and 6-ZGNR perform the best. 4-ZGNR has the highest MR of 3300% at 0.3 V, and 6-ZGNR has the second highest MR of 3100% at 0.05 V. The highest room-temperature MR obtained in the second-type ZGNR-based spin-valve is much lower than the highest MR in the first-type ZGNR-based spin

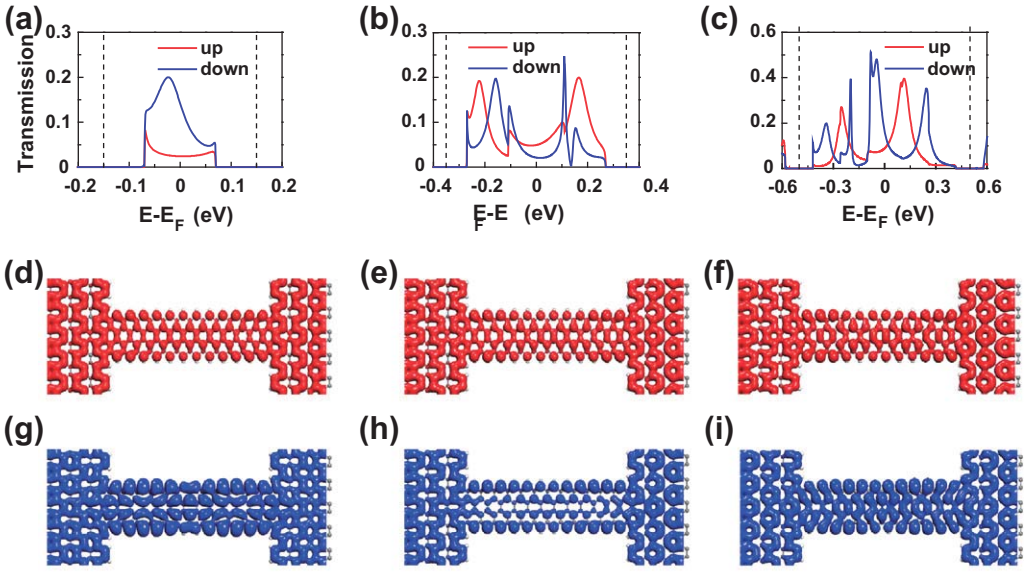

Fig. 3. 4-ZGNR in the FM configuration. (a) Spin-polarized transmission spectra at V_{bias} = 0.3 V, (b) V_{bias} = 0.7 V and (c) V_{bias} = 1.0 V. Dashed black lines denote the bias window. Isosurfaces of (d) spin-up LDOS at V_{bias} = 0.3 V, (e) spin-up LDOS at V_{bias} = 0.7 V, (f) spin-up LDOS at V_{bias} = 1.0 V, (g) spin-down LDOS at V_{bias} = 0.03 V, (h) spin-up LDOS at V_{bias} = 0.7 V, and (i) spin-down LDOS at V_{bias} = 1.0 V at the Fermi level. Isovalues of the LDOS are 5×10^{-4} a.u.

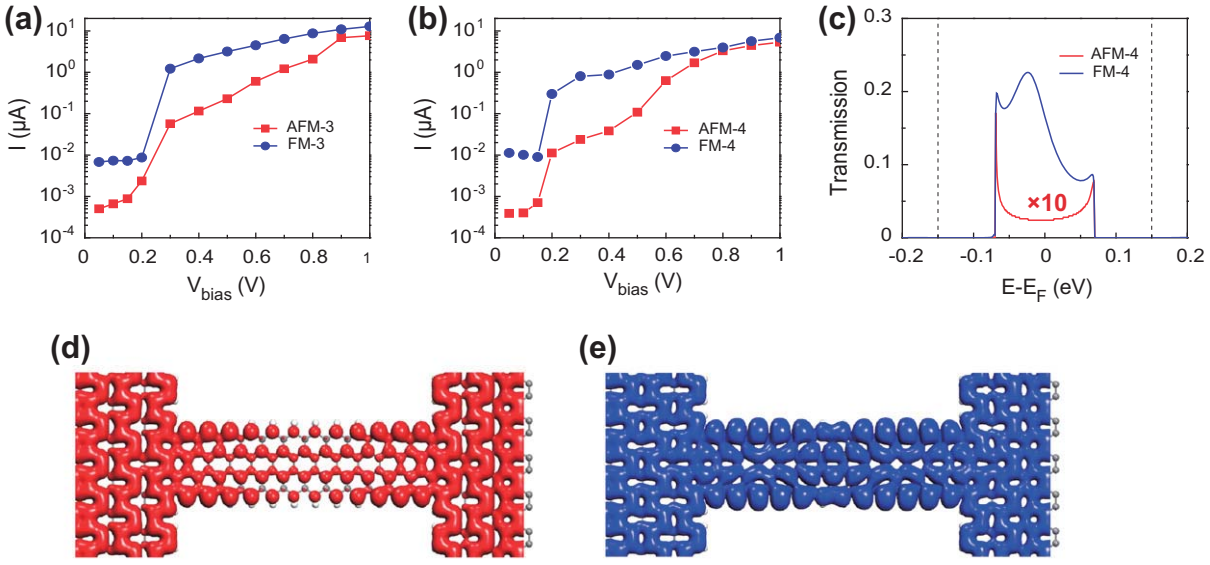

Fig. 4. *I–V* characteristics of the (a) AFM-coupled 3-ZGNR and (b) the FM-coupled 4-ZGNR. (c) Total transmission spectra of the AFM- and FM-coupled 4-ZGNR at V_{bias} = 0.3 V. The transmission spectrum of the AFM-coupled case (red line) is augmented by 10 times. (d) Isosurfaces of the total LDOS of (d) the AFM-coupled 4-ZGNR and (e) the FM-coupled 4-ZGNR at the Fermi level under V_{bias} = 0.3 V. Isovalues of the LDOS are 5×10^{-4} a.u. (For interpretation of the references to colour in this figure legend, the reader is referred to the web version of this article.)

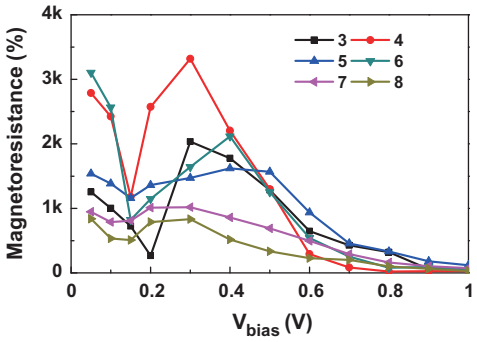

Fig. 5. Magnetoresistances of different-width ZGNRs as a function of bias at 300 K.

valve (1 million percent for H-saturated ZGNR device [12] and 1 billion percent for bare ZGNR device [13]). The maximum experimental room-temperature MR values are at a few hundred percent [14,19–22], and our theoretical maximum MR in the second-type ZGNR-based spin-valve remains one order of magnitude much larger than the available experimental values.

Due to the semiconducting nature of the AFM configuration, the transport of the AFM configuration is a tunneling phenomenon. While the ribbon length increases, the tunneling is suppressed. At the same time, the metallic transport of the FM configuration is almost unchanged. Consequently the MR is generally favored as the ribbon length gets larger [15].

The critical magnetic field needed to change the spin polarization from an anti-parallel to a parallel configuration of a given graphene nanoribbon is reduced as the temperature drops, since it is determined by the spin correlation length [15]. Munoz-Rojas et al. [15] calculated that this critical magnetic field is 0.03 T at liquid He temperature, which is easily attained in the laboratory.

4. Conclusions

In conclusion, we study the transport properties of a ZGNR seamlessly joining two half-planar graphene electrodes. We find that the AFM coupled asymmetrical ZGNRs and the FM coupled symmetrical ZGNRs show remarkable sign-changeable (with bias) spin-filter efficiency. These devices have outstanding giant magnetoresistance at finite bias. The maximum room-temperature MR we obtain is one order of magnitude larger than the recent experimental results. Based on these remarkable characteristics, our devices have potential application in spintronics.

Acknowledgements

This work was supported by the NSFC (Grant Nos. 10774003, 10474123, 10434010, 90626223, and 20731162012), National 973 Projects (Grant No. 2007CB936200, MOST of China), Fundamental Research Funds for the Central Universities, Program for New Century Excellent Talents in University of MOE, and National Foundation for Fostering Talents of Basic Science (Grant No. J0630311) of China.

Appendix A. Supplementary data

Supplementary data associated with this article can be found, in the online version, at doi:10.1016/j.commatsci.2011.05.004.

References

[1] C. Berger, Z.M. Song, T.B. Li, X.B. Li, A.Y. Ogbazghi, R. Feng, Z.T. Dai, A.N. Marchenkov, E.H. Conrad, P.N. First, W.A. de Heer, J. Phys. Chem. B 108 (2004) 19912.
[2] K.S. Novoselov, A.K. Geim, S.V. Morozov, D. Jiang, Y. Zhang, S.V. Dubonos, I.V. Grigorieva, A.A. Firsov, Science 306 (2004) 666.
[3] K.S. Novoselov, A.K. Geim, S.V. Morozov, D. Jiang, M.I. Katsnelson, I.V. Grigorieva, S.V. Dubonos, A.A. Firsov, Nature 438 (2005) 197.
[4] C. Berger, Z.M. Song, X.B. Li, X.S. Wu, N. Brown, C. Naud, D. Mayou, T.B. Li, J. Hass, A.N. Marchenkov, E.H. Conrad, P.N. First, W.A. de Heer, Science 312 (2006) 1191.
[5] A.K. Geim, K.S. Novoselov, Nat. Mater. 6 (2007) 183.
[6] K.S. Novoselov, S.V. Morozov, T.M.G. Mohinddin, L.A. Ponomarenko, D.C. Elias, R. Yang, I. Barbolina, P. Blake, T.J. Booth, D. Jiang, J. Giesbers, E.W. Hill, A.K. Geim, Electronic properties of graphene, in: 21st International Winterschool on Electronic Properties of Novel Materials, 2007, Kirchberg, Austria.
[7] E.W. Hill, A.K. Geim, K. Novoselov, F. Schedin, P. Blake, IEEE Trans. Magn. 42 (2006) 2694.

[8] W.H. Wang, K. Pi, Y. Li, Y.F. Chiang, P. Wei, J. Shi, R.K. Kawakami, Phys. Rev. B 77 (2008) 020402.
[9] M. Fujita, K. Wakabayashi, K. Nakada, K. Kusakabe, J. Phys. Soc. Jpn. 65 (1996) 1920.
[10] Y.W. Son, M.L. Cohen, S.G. Louie, Nature 444 (2006) 347.
[11] Y.W. Son, M.L. Cohen, S.G. Louie, Phys. Rev. Lett. 97 (2006) 216803.
[12] W.Y. Kim, K.S. Kim, Nat. Nanotechnol. 3 (2008) 408.
[13] R. Qin, J. Lu, L. Lai, J. Zhou, H. Li, Q.H. Liu, G.F. Luo, L.N. Zhao, Z.X. Gao, W.N. Mei, G.P. Li, Phys. Rev. B 81 (2010) 233403.
[14] J.W. Bai, R. Cheng, F.X. Xiu, L. Liao, M.S. Wang, A. Shailos, K.L. Wang, Y. Huang, X.F. Duan, Nat. Nanotechnol. 5 (2010) 655.
[15] F. Munoz-Rojas, J. Fernandez-Rossier, J.J. Palacios, Phys. Rev. Lett. 102 (2009) 136810.
[16] C.H. Jin, H.P. Lan, L.M. Peng, K. Suenaga, S. Iijima, Phys. Rev. Lett. 102 (2009) 205501.
[17] K. Wakabayashi, M. Sigrist, Phys. Rev. Lett. 34 (2000) 3390.
[18] Z.Y. Li, H.Y. Qian, J. Wu, B.L. Gu, W.H. Duan, Phys. Rev. Lett. 100 (2008) 206802.
[19] S.S.P. Parkin, C. Kaiser, A. Panchula, P.M. Rice, B. Hughes, M. Samant, S.H. Yang, Nat. Mater. 3 (2004) 862.
[20] S. Yuasa, T. Nagahama, A. Fukushima, Y. Suzuki, K. Ando, Nat. Mater. 3 (2004) 868.
[21] S. Ikeda, J. Hayakawa, Y. Ashizawa, Y.M. Lee, K. Miura, H. Hasegawa, M. Tsunoda, F. Matsukura, H. Ohno, Appl. Phys. Lett. 93 (2008) 082508.
[22] D.L. Sun, L.F. Yin, C.J. Sun, H.W. Guo, Z. Gai, X.G. Zhang, T.Z. Ward, Z.H. Cheng, J.A. Shen, Phys. Rev. Lett. 104 (2010) 236602.
[23] ATOMISTIX Toolkit version 2008.10. QuantumWise A/S. <www.quantumwise.com>.
[24] J. Taylor, H. Guo, J. Wang, Phys. Rev. B 63 (2001) 245407.
[25] M. Brandbyge, J.L. Mozos, P. Ordejon, J. Taylor, K. Stokbro, Phys. Rev. B 65 (2002) 165401.
[26] H.J. Monkhorst, J.D. Pack, Phys. Rev. B 13 (1976) 5188.
[27] J.P. Perdew, J.A. Chevary, S.H. Vosko, K.A. Jackson, M.R. Pederson, D.J. Singh, C. Fiolhais, Phys. Rev. B 46 (1992) 6671.
[28] S. Datta, Electronic Transport in Mesoscopic Systems, Cambridge University Press, Cambridge, England, 1995.
[29] M. Ezawa, Phys. Rev. B 73 (2006) 045432.
[30] L. Yang, C.H. Park, Y.W. Son, M.L. Cohen, S.G. Louie, Phys. Rev. Lett. 99 (2007) 186801.
[31] S.A. Crooker, M. Furis, X. Lou, C. Adelmann, D.L. Smith, C.J. Palmstrom, P.A. Crowell, Science 309 (2005) 2191.
[32] X.H. Lou, C. Adelmann, S.A. Crooker, E.S. Garlid, J. Zhang, K.S.M. Reddy, S.D. Flexner, C.J. Palmstrom, P.A. Crowell, Nat. Phys. 3 (2007) 197.
[33] A.N. Chantis, K.D. Belashchenko, D.L. Smith, E.Y. Tsymbal, M. van Schilfgaarde, R.C. Albers, Phys. Rev. Lett. 99 (2007) 196603.
[34] L. Wang, X.F. Gao, X. Yan, J. Zhou, J. Lu, Z.X. Gao, S. Nagase, S. Sanvito, Y. Maeda, T. Akasaka, W.N. Mei, J. Phys. Chem. C 114 (2010) 21893.